



## Late Holocene rupture history of the Ventas de Zafarraya Fault (Southern Spain)

### *Historia de la ruptura de la Falla de Ventas de Zafarraya durante el Holoceno Tardío*

Grützner, C. <sup>(1)</sup>; Ruano, P. <sup>(2,3)</sup>; Jabaloy, A. <sup>(2)</sup>; Galindo-Zaldívar, J. <sup>(2,3)</sup>; Becker-Heidmann, P. <sup>(4)</sup>; Sanz de Galdeano, C. <sup>(3)</sup>; Rudersdorf, A. <sup>(1)</sup>; Reicherter, K. <sup>(1)</sup>

(1) Neotectonics and Natural Hazards, RWTH Aachen University, Lochnerstr. 4-20, 52056 Aachen, Germany, c.gruetzner@nug.rwth-aachen.de

(2) Departamento de Geodinámica, Univ. Granada, Campus Fuentenueva, E-18071 Granada, Spain

(3) Instituto Andaluz de Ciencias de la Tierra (CSIC-Univ.Granada), Facultad de Ciencias, Univ. Granada, 18071 Granada, Spain

(4) Institut für Bodenkunde, Univ. of Hamburg, Germany

### Resumen

Uno de los terremotos más destructivos ocurridos en la Península Ibérica tuvo lugar en la Falla de Ventas de Zafarraya (VZF, Granada, Sur de España) en AD 1884 ( $M_s$  6.7). Nuevos datos paleosismológicos basados en el análisis de trincheras de falla y dataciones radiométricas permiten reconstruir la historia sísmica de la VZF durante los últimos 10 ka. Se han reconocido cuatro grandes eventos paleosísmicos (c. 6,5 + 0,5 Ms) que pueden considerarse como el terremoto máximo posible en la VZF. Una de las principales conclusiones es que el periodo de recurrencia de estos “terremotos característicos” se encuentra entorno a los 2000 años. Dada estas elevadas tasas de recurrencia, las investigaciones futuras deberían enfocarse hacia otras fallas de longitud y tasas de actividad similares ya que estas pueden presentar una importante peligrosidad sísmica durante un futuro cercano.

**Palabras Clave:** Paleosismología, Falla de Ventas de Zafarraya, Terremoto de 1884, Cordillera Bética, España.

### Abstract

One of the most destructive earthquakes on the Iberian Peninsula ( $M_s$  6.7) occurred in 1884 along the Ventas de Zafarraya Fault (VZF, southern Spain). New paleoseismological data based on trenching and radiometric dating allow the faulting history in the last 10 ky to be characterized. Four major events ( $M_s$  around 6.5 ± 0.5) are revealed, which are regarded as maximum credible earthquakes along the fault. The mean slip rate during



the Holocene is estimated to be on the order of 0.3 to 0.45 mm/y. One major conclusion is that the recurrence period for “characteristic” earthquakes along the VZF is on the order of 2000 years. Due to these expected recurrence rates, future research should now focus on other faults of similar length and activity, because those faults will be posing a seismic hazard for the Iberian Peninsula in the near future.

**Key words:** Paleoseismology, Ventas de Zafarraya Fault, 1884 Earthquake, Betic Cordillera, Spain.

## 1. Introduction

Paleoseismicity and the effects of historical earthquakes which occurred in the western Gibraltar Arc and Betic Cordilleras have been studied for more than 25 years (Sanz de Galdeano, 1985). The importance of seismicity in the southern part of the Iberian Peninsula was, however, recognized much earlier (e.g., Muñoz and Udías, 1980). The number of paleoseismic studies in this area increased significantly during the last 15 years, although they were restricted to some major faults (Alhama de Murcia Fault: Silva *et al.*, 2003; Masana *et al.* 2004, 2005; Martínez-Díaz *et al.*, 2010a,b; Carboneras Fault: Moreno *et al.*, 2010) and especially in areas where known historical events have taken place (VZF and Granada Basin: Reicherter, 2001; Reicherter *et al.*, 2003; Sanz de Galdeano *et al.*, 2003; Rodríguez Peces *et al.*, 2010; Bajo Segura fault Zone: Alfaro *et al.*, 2001, 2012; Campo de Gibraltar: Grützner *et al.*, 2012, amongst other authors and areas). A further major step was achieved by setting up the Quaternary Active Faults Database of Iberia (QAFI v.2.0), which has recently been published (García-Mayordomo *et al.*, 2012).

The most destructive earthquake of the Iberian Peninsula during the last 150 years occurred on the evening of Christmas Day 1884 at 09:08 pm (“Terremoto de Andalucía”) in southern Spain, and was felt roughly between Málaga and Granada (Fig. 1). More than 800 casualties were caused and several villages were reported to have been destroyed. According to the greatest damage, the epicenter was probably located between Arenas del Rey and Ventas de Zafarraya (Muñoz and Udías, 1980). During the earthquake a 15 to 17 km long surface rup-

ture opened at the Ventas de Zafarraya Fault (VZF) with a maximum vertical displacement of around 1.5 m; open fissures and cracks were associated with the rupture as well as lateral spreading, landslides and liquefaction.

The maximum intensity was MSK X (Mercalli-Sponheuer-Karnik scale) from which a magnitude of 6.5 - 7 has been calculated (Muñoz and Udías, 1980). European commissions studying the earthquake effects have described a complex pattern of surface cracks, landslides, rock falls, liquefaction, and changes in the spring water chemistry and temperature associated with the seismic event (see EEE INQUA Scale reports for Spain, Silva *et al.*, 2009). The international collaboration resulted in the reconstruction of the village of Arenas del Rey with one of the first earthquake-safe designs (for more information see Martínez Solares, 2011).

Although no unambiguous primary fault-related surface ruptures or coseismic movements along the fault plane were recognized, Muñoz and Udías (1980) and Sanz de Galdeano (1985) concluded that the earthquake was possibly associated with several faults and tectonic blocks along the northern margin of the Sierra Tejeda (Fig.1B). This seems quite reasonable as morphometric studies and trenching investigations revealed evidence for surface rupturing. The structural and neotectonic characteristics of the VZF in the structural framework of the Betic Cordilleras were described by Galindo-Zaldívar *et al.* (2003) and quite recently, the Zafarraya Polje has been related to dextral strike-slip faults and associated normal faulting (Sanz de Galdeano, 2012). Preliminary investigations on the paleoseismicity of the Ventas de Zafarraya were conducted by a Spanish-German team (Reicherter, 2001; Reicherter *et al.*, 2003). A

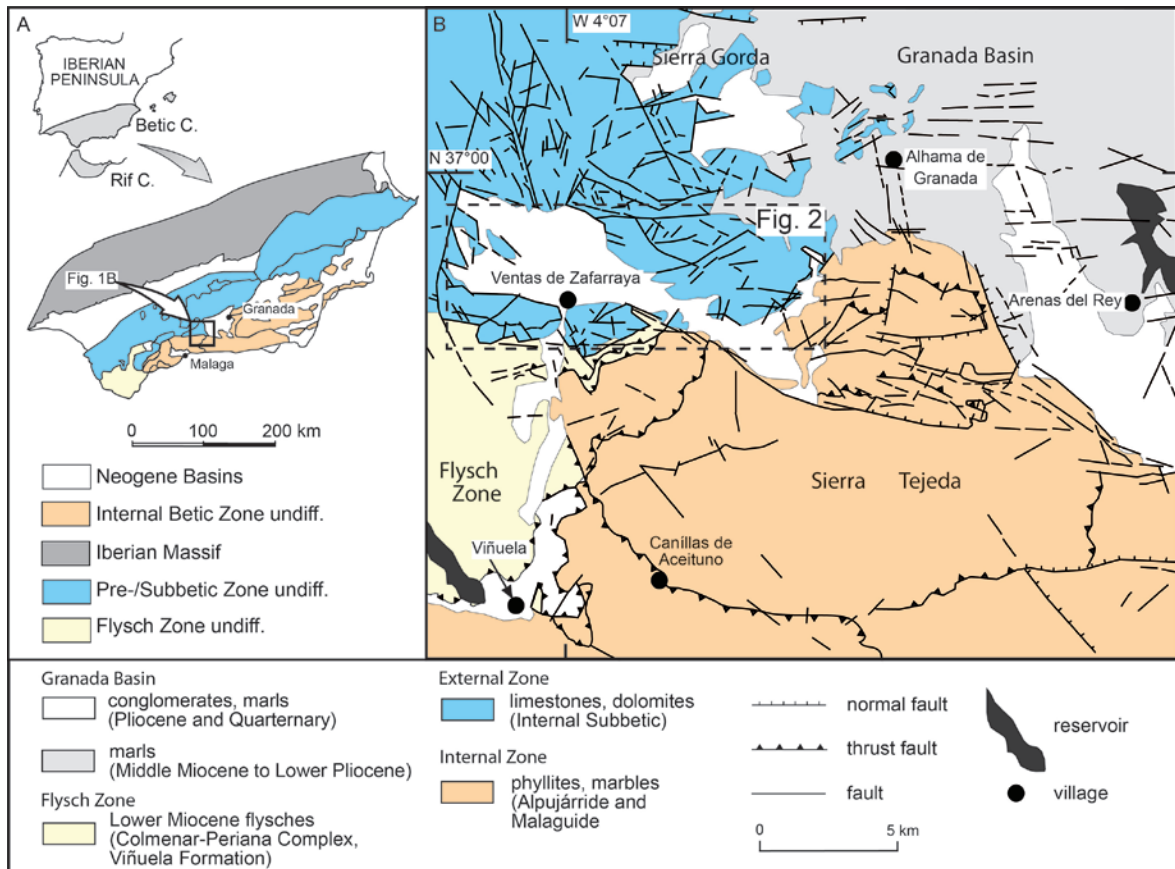


Figura 1. A) Esquema simplificado de las unidades geológicas y estructurales de la Cordillera Bética en Andalucía. B: Esquema Geológico y estructural de la parte Sur de la Cuenca de Granada y del Poljé de Zafarraya.

Figure 1. A) Simplified geological and structural units of the Betic Cordilleras in Andalusia. B: Geological and structural map of the southern Granada Basin and Zafarraya Polje.

catalogue of historical earthquakes and active faults of the Betic Cordilleras has been compiled and is available online (e.g., IGN, 2012; García-Mayordomo *et al.*, 2012). According to seismic maps provided by the IGN (2012), the area of the 1884 VZF earthquake is the area of highest seismic hazard in Spain with expected ground accelerations larger than 0.16 g. New trenching data and radiocarbon dates obtained along the VZF are presented in this paper.

## 2. Paleoseismic study of the Ventas de Zafarraya Fault

The western segment of the Ventas de Zafarraya Fault (VZF) has been characterized on the basis of trenching studies carried out

in the fall of 2004. The major objective was to obtain more reliable ages for faulting and to extend and check the earthquake history reported by Reicherter *et al.* (2003). This was because the authors' investigated outcrop in a cemetery no longer exists, and it was also of limited extent (both in depth and length). In order to analyze the paleoseismic faulting history of the VZF and to study its relationship with the 1884 earthquake and other previous seismic events along the same fault, three trenches were opened perpendicular to the E-W striking fault plane. All trenches were situated W of Ventas de Zafarraya along the northern slope of the Sierra Alhama mountain front (Fig. 2). After documentation and sampling the trenches were closed again, with the exception of trench 1 and its western

wall, which is still accessible but on private property. The investigations included sedimentology, microstratigraphy, and  $^{14}\text{C}$ -dating. Furthermore, an evaluation of aerial and satellite imagery, morphotectonic analysis and an assessment of the recent and historical seismicity was undertaken, as well as high-resolution sub-surface Ground-Penetrating Radar (GPR). The stratigraphic relationships along the active VZF permit the reconstruction of the faulting history, including the number and relative size of faulting events, and the determination of recurrence intervals.

## 2.1. Morphotectonic analysis

To investigate morphotectonic features of this area, a digital elevation model (DEM) was produced based on vectorized data from the Junta de Andalucía (ICA, 2012). Digitized 10 m contour lines allow an adequate resolution to perform a morphotectonic analysis. Bull and McFadden (1977) introduced the mountain front sinuosity index (*smf*), which investigates the mountain front - piedmont junction to assess tectonic activity. Basin-delimiting faults that overprint mountain

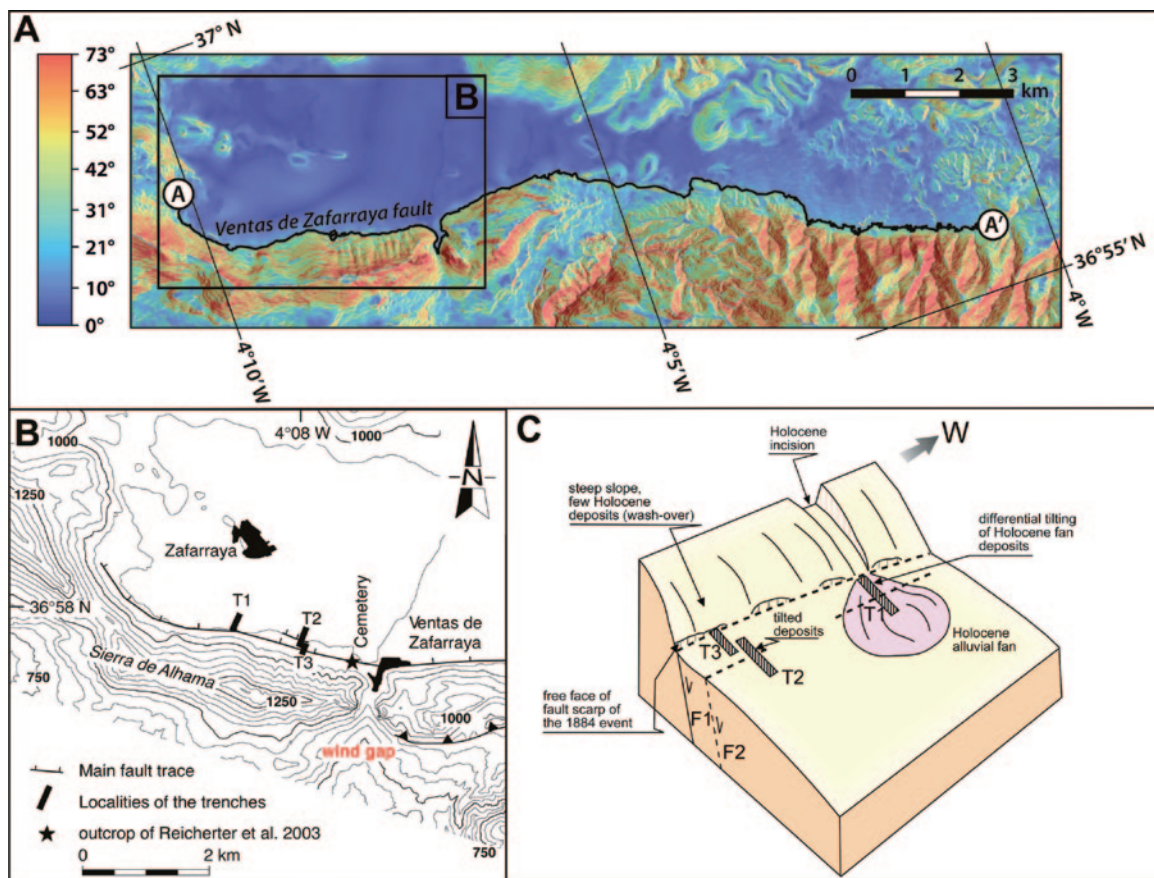


Figura 2. A) Mapa de pendientes de la zona Sur del Polje de Zafarraya. La línea A-A' indica la zona de frente montañoso investigada entre el polje y Sierra Tejada para el cálculo del índice Smf. Note el claro contraste existente entre las altas pendientes de la Sierra ( $< 73^\circ$ ) y la superficie plana del polje. B) mapa topográfico del Polje de Zafarraya indicando la localización de las trincheras de fallas (Modificado de Reichert *et al.*, 2003). C) Esquema de las características morfoestructurales más importantes de la falla en relación a la localización de las trincheras.

Figure 2. A) Slope angle map of the southern Zafarraya polje. Line A-A' indicates the investigated mountain front - piedmont junction between the polje and the Sierra de Alhama and Sierra Tejada for the mountain front sinuosity *smf* calculation. Note the clear contrast between the steep Sierras with slopes up to  $73^\circ$  and the flat basin surface. B) Topographic map of the Zafarraya Polje with trenching sites (modified from Reichert *et al.*, 2003). C) Sketch of the morphotectonic features and location of the trenches along the Ventas de Zafarraya Fault.

relief create and maintain rather straight mountain fronts, whereas non-tectonic or inactive mountain fronts form highly irregular and lobate forms due to river incision and sediment accumulation (Mayer, 1986; Silva *et al.*, 2003; Bull, 2007). The *smf* index can, therefore, be determined as the ratio of the length of the mountain front - piedmont junction (*Lmf*) to the straight connection between the end points of the observed structure (*Ls*). Low values down to 1 correspond to straight mountain fronts and give evidence for an tectonically active structure, whereas erosion-dominated mountain fronts exhibit high *smf* values, usually up to 3-7 (Bull and McFadden, 1977; Bull, 2007). The mountain front-piedmont junction was identified by the computation of slope angle contrasts and slope aspects through automated processing steps. In this way selection bias was omitted and the overestimation of mountain front straightness could be avoided. The investigated length of the mountain front *Lmf* amounts to 23,259 m and *Ls* is 15,004 m (Fig. 2A). The sinuosity of the northern Sierra de Alhama and Sierra Tejada mountain front is *smf* = 1.55, which can be classified as an active tectonic structure after Bull and McFadden (1977) and Silva *et al.* (2003). Tectonic activity is also demonstrated quite nicely by a beautiful “wind gap” (Fig. 2B). This is a former river course which once drained the karstic polje, but now is closed and shut down by footwall uplift forming an endorheic basin. The digital elevation model and series of aerial photos have also been used to identify possible trenching sites where the slopes of the Sierra de Alhama are not too steep (along the shallower slopes more talus sediment and colluvium has accumulated, Fig. 2C).

## 2.2. Ground Penetrating Radar

Ground penetrating radar (GPR) was used prior to excavations to identify promising trench sites. After trenching, GPR was applied in order to verify that sedimentary features found in the trenches are not restricted to a

single location only, but can be found along the entire fault zone. The method was also used to allow lateral correlation of features between the trench sites.

The GSSI SIR-2 data acquisition system and a 200 MHz antenna with survey wheel were used for the GPR survey in 2004. 14 profiles were collected perpendicular to the VZF, eight of which in the immediate vicinity of the trenches. Penetration depths between 3 m and 8 m were achieved depending on the location. Spatial resolution is on the order of 0.1 m to 0.2 m. Data processing was done with ReflexW software (<http://www.sandmeier-geo.de/reflexw.html>). Its workflow included dewow, background removal, frequency filtering, gain adjustment, averaging and topography correction. Since the data were not migrated, diffraction hyperbolae are still visible and dipping angles appear shallower than they really are.

Several profiles at the location of trench 1 were recorded before its excavation (Fig. 2C). Profile 60 was collected at the later position of the trench (see the grey outline in figure 3A). Several diffraction hyperbolae in the radar-gram are caused by boulders with a diameter greater than 0.2 m, but not every boulder does result in a clear hyperbola due to superimposition. Reflectors inclined towards the fault can be associated with corresponding layers in the trench log. Interestingly, GPR data show more inclined layers than in the trench log and allow lateral correlations. High amplitudes occur at gravel layers, since the electromagnetic contrast is strong in this case; low electrical resistivity of the fine-grained matrix leads to a shallow penetration depth of only 3 m. Parallel profiles show similar features like profile 60.

Profile 67 was recorded in order to find out a promising location for trench 3. It covers the entire excavation site and reveals geological features to a depth of 8 m (Fig. 3). Large boulders cause hyperbolae and gravel accumulations result in strong reflections, especially in the northern part of the profile. Hyperbolae can be observed to a depth of 6 m; the deepest ones have not been marked

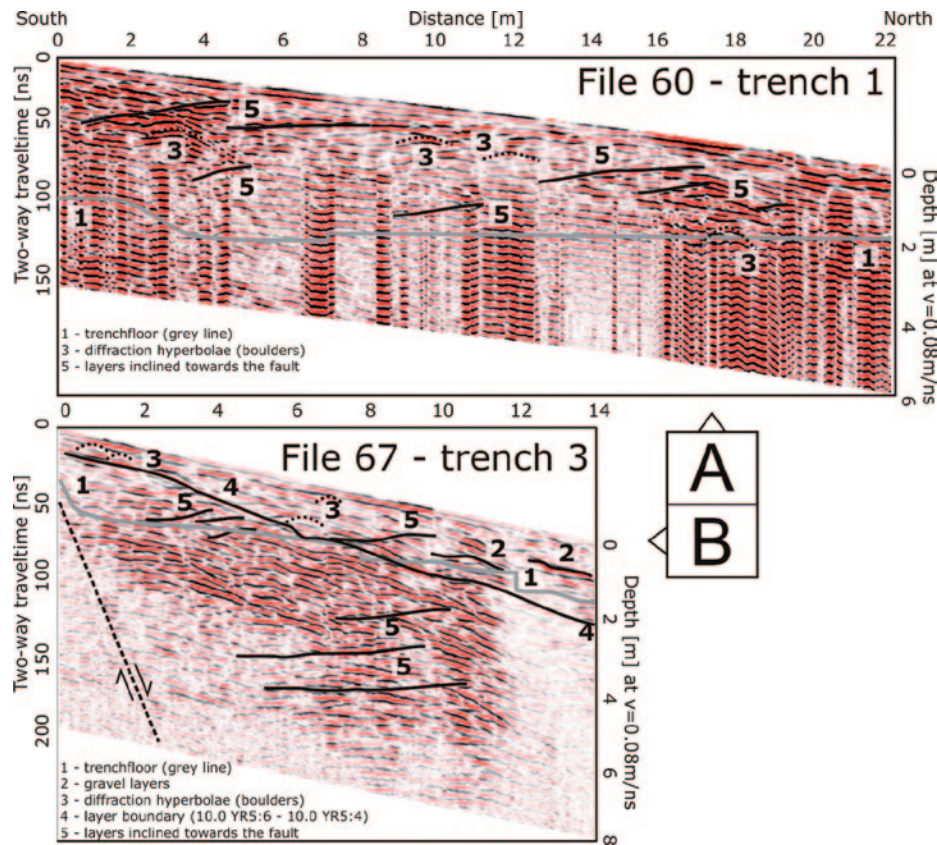


Figura 3. Datos Georadar de las trincheras. A) El perfil GPR 60 se realizó sobre la posición de la antigua trinchera 1 e ilustra la ocurrencia de hipérbolas de difracción asociadas con caídas de bloques (sísmicamente inducidas?) y estratos buzando hacia el plano de falla. B) El perfil GPR 67 se realizó previo a la excavación de la trinchera 3 y muestra similares características que el anterior sugiriendo deformaciones de los depósitos relacionadas con la falla.

Figure 3. Radar data from the trenches. A) GPR Profile 60 was recorded at the later location of trench 1 and reveals diffraction hyperbolae associated with (seismically induced?) rockfall boulders and layers dipping towards the fault plane. B) GPR Profile 67 was recorded before the excavation of trench 3 and shows similar features clearly indicating fault-related sediment deformation.

in Fig. 3 in order not to obscure the structures found there. A slight change in reflection intensities marks the boundary between two layers that can be distinguished by different colors in the trench log. GPR data reveal that the uppermost layer thickens from 1 m at the fault plane to more than 2 m in a distance of 14 m. The dipping angle of the layer boundary does not change. Layers with an inclination towards the fault can be observed from 1 m to 5 m depth. They appear to have the same dipping angle. While the shallowest ones can be correlated to the trench log, geophysical data reveal the geometry of the deformed sediments in depths inaccessible to excava-

tions. Profiles parallel to 67 image similar features along the fault zone.

As the trenches were planned in the hanging wall of the VZF, the fault trace was not crossed by radar. As a result, it is possible to detect locations with varying sediment thicknesses. Based on these variations the most promising trenching sites were chosen.

### 2.3. Trenching and dating

The location of trench 1 was evaluated by GPR and field mapping (Fig. 2B). It is situated in a Holocene alluvial fan, providing sufficient

sediment thicknesses. Trench 1 is c. 22 m in length and max. 4.5 m deep. The SSW end is directly situated at the limestone fault scarp of the VZF, which has a height of approx. 1 m. After machine-driven excavation and hand cleaning, a 1 by 1m grid was set up on the western trench wall. After photographing and sketching at 1:5 scale, grain-size, color (after Munsell, 1990; see Fig. 4), faults and litho-units were determined. Later, sample points for  $^{14}\text{C}$  dating were chosen. All samples were taken from material of the colluvial wedges (paleosols). A total of 8 samples was collected

and dated. Trench 2 and 3 are located to the East of trench 1 (Fig. 2B and C) and overlap each other. Trench 2 had a length of 12 m and a depth of 3 m, trench 3 was 14 m long and up to 2 m deep. The SSE end of trench 3 is located against the bedrock fault scarp created during the 1884 rupture. Trenches 2 and 3 were processed similar to trench 1. Three samples were taken from trench 2 but not dated, and one sample was dated from trench 3 (Fig. 4).

Trenches 1 and 3 revealed several hints for tectonic activity and earthquake-related sedi-

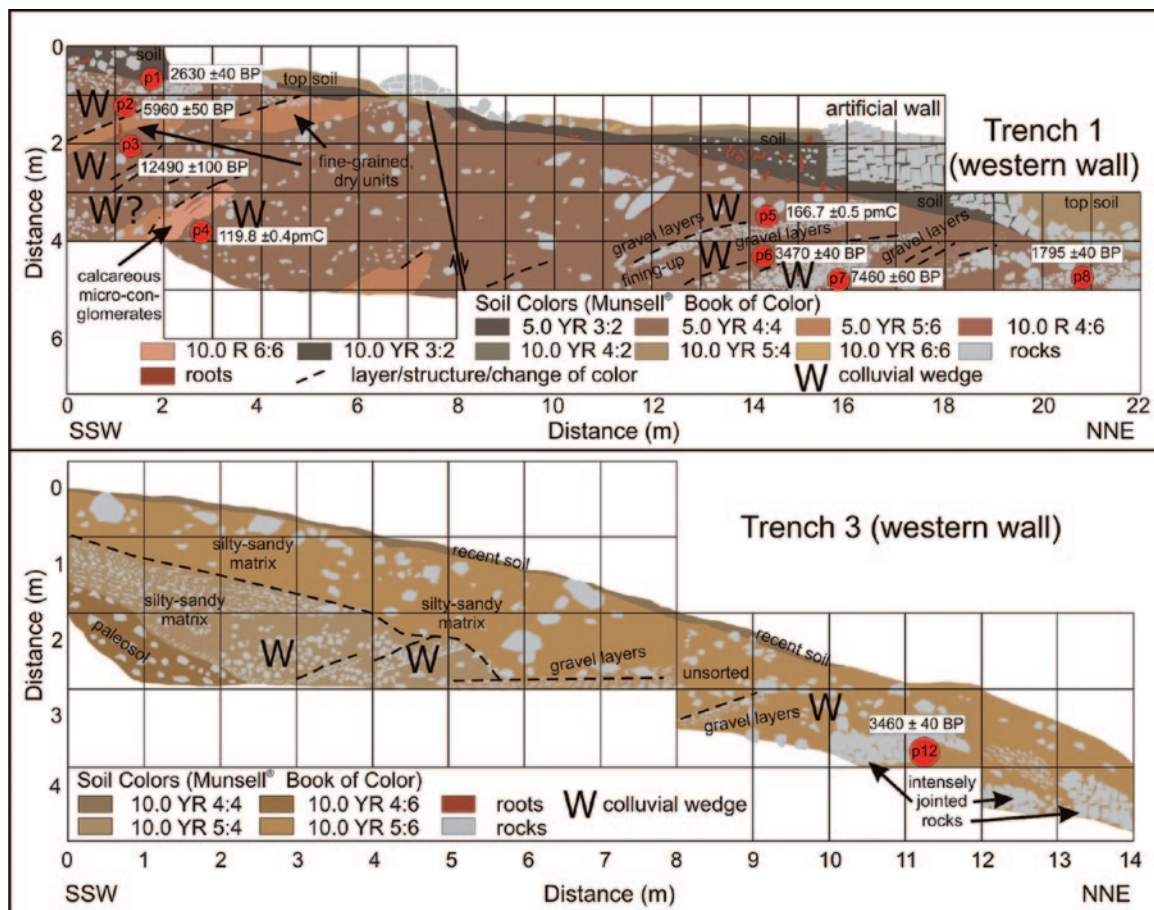


Figura 4. Log de la pared oeste de la trinchera 1 (arriba). Log de la pared oeste de la trinchera 3 (abajo). Se observa la localización de las muestras de  $^{14}\text{C}$ , así como la inclinación hacia el sur de los diferentes estratos y capas en ambas trincheras. Tres cuñas coluviales (W) principales se identifican y muestrean para  $^{14}\text{C}$  en la trinchera 1 (muestras p1-p4).

Una falla secundaria desarrolla un conjunto similar de tres cuñas coluviales en la mitad de la trinchera, también muestreadas (muestras p5-p7).

Figure 4. Trench log of trench 1 western wall (upper figure). Trench log of trench 3 western wall (lower figure). Note sample locations of radiocarbon dating and southward tilt and inclination of layers and stratification in both trenches. A set of three main colluvial wedges (W) was identified and sampled for  $^{14}\text{C}$  dating in trench 1, corresponding to sample p1-p4. A set of three wedges developed at a secondary fault in the middle of the trench, with the relevant samples being p5-p7.

mentary features. The occurrence of sediment layers in the hanging wall inclined towards the fault clearly indicates a rotation of the layers due to a faulting event. Without tectonic movement the layers would have been horizontally or inclined in slope direction. After being co-seismically downthrown, colluvial wedges can form, distinctively marked by gravels. These gravels and boulders might be related to earthquake induced rockfalls. In any case they mark a phase of intensified deposition and filling of the wedge. At least 3 generations of those wedges were identified in trench 1 and dated (samples p1-p4, table 1), with the lower wedges dipping steeper due to repeated coseismic rotation. This is also proven by GPR data. A secondary fault located 8 m away from the main fault plane led to the development of another set of wedges in the northern part of trench 1 (samples p5-p7). No surface topographic expression of the secondary fault can be found due to the fast erosion of the rather soft material. In trench 3, similar inclined gravel layers could be identified. This proves that they occur not only locally but along the fault, thus, being related to fault activity. One wedge of trench 3 was also dated. The formation of the colluvial wedges was assigned to single earthquake events, so that the dates from the samples can be considered representing the period right after the seismic event (Fig. 5). Event 3 is questionable and may be more or less coeval to event 4, and hence event 3 and 4 may reflect the same event. The large

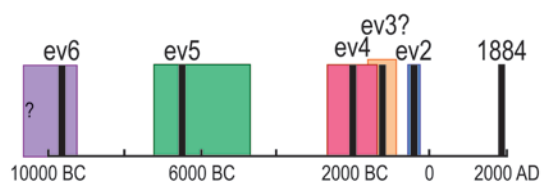


Figura 5. Periodicidad de los eventos sísmicos registrados en la Falla de Ventas de Zafarraya, incluyendo los datos e interpretaciones de Reicherter *et al.* (2003). Los eventos 3 y 4 son prácticamente contemporáneos, seguramente se trata de un solo evento. Los grandes márgenes de error asociados al evento 5 son debidos a la poca calidad del material datado. El evento 6 es más antiguo que 9500 BP, ya que esta fecha representa su edad mínima.

Figure 5. Timing of earthquake events found along the Ventas de Zafarraya Fault, including the data and interpretation of Reicherter *et al.* (2003). Event 3 is more or less coeval to event 4, or they may be one single event. Large dating errors for event 5 are due to unsuitable dating material. Event 6 is older than 9500 BP since the date represents a minimum age.

error in precise dating of event 5 is due to unsuitable dating material (sandy sediment with low content of organic carbon). Event 6 is definitively older than 9500 BP (minimum age). The thickness of the wedges is limited by the actual coseismic offset during the respective earthquake. In our case the wedges do not exceed 1 m thickness. Wells and Coppersmith relationships (Wells and Coppersmith, 1994) for magnitude vs. displacement would allow assigning a magnitude of not more than 6.7 for the events, which is in correspondence with the values retrieved for magnitude vs. rupture length.

Tabla 1. Resultados  $^{14}\text{C}$ .  
Table 1.  $^{14}\text{C}$  dating results.

lab number	sample	material	uncalibrated $^{14}\text{C}$ age	location
HAM-3833	P1	paleosol	2630 ± 40 BP	Trench 1, grid B1
HAM-3834	P2	paleosol	5960 ± 50 BP	Trench 1, grid B2
HAM-3835	P3	paleosol	12490 ± 100 BP	Trench 1, grid B3
HAM-3836	P4	paleosol	119,8 ± 0,4 pmC	Trench 1, grid C4
HAM-3837	P5	paleosol	166,7 ± 0,5 pmC	Trench 1, grid O4
HAM-3838	P6	paleosol	3470 ± 40 BP	Trench 1, grid O5
HAM-3839	P7	paleosol	7460 ± 60 BP	Trench 1, grid P5
HAM-3840	P8	paleosol	1795 ± 40 BP	Trench 1, grid U5
HAM-3844	P12	paleosol	3460 ± 40 BP	Trench 3, west, grid L4

### 3. Conclusions

The paleoseismological investigations along this segment of the VZF demonstrate that coseismic displacements have occurred, not only during but also prior to the 1884-earthquake. Repeated colluvial wedges along fault scarps, and their stratigraphic relation with slope wash sediments and paleosols preserved within the half-graben, provide evidence for an earthquake-related faulting. Episodic rotation towards the fault plane is observed. Paleoseismic and radiocarbon data allow inferring that at least two pre-1884 ruptures occurred on the fault during the last 10 ky.

The data yield supplementary information detailing average earthquake recurrence intervals of 2 to 3 ky for large earthquakes of  $M > 6.5$ , under the assumption of uniform return periods (Schwartz and Coppersmith, 1984). Taking into account that the vertical offset on the fault is about 1,500 m, and considering that the fault system is most likely post-Tortonian in age (Reicherter and Peters, 2005) it is possible to estimate that the minimum mean slip rate of the fault is 0.17 mm/y. The Holocene slip rate was estimated between 0.30 and 0.45 mm/y. This is typical for faults with a moderate earthquake activity. If the empirical dePolo and Slemmons (dePolo and Slemmons, 1990) relationships are considered, these data suggest a mean recurrence interval of about 2000 years on the studied segment of the Ventas de Zafarraya Fault (Fig. 5). It is, therefore, one of the major active faults in southern Spain.

Regarding the study area along the VZF in the western depression linked to the Granada Basin, where results were first published in 2003, three surface rupturing earthquakes in the last 8.8 ky were found (Reicherter *et al.*, 2003). Later, trenching studies were conducted at two sites and three new trenches were opened (this study). Evidence for all together at least 5-6 major events during the Holocene at the VZF was found. The events did most probably not exceed the magnitude of the 1884-earthquake ( $M 6.7$ ). This supports the previous

idea that the fault is only capable to produce a  $M_{max}$  of  $< 7$ . The recurrence period for earthquakes of this order is approx. 2000 years. The Ventas de Zafarraya Fault constitutes an active and potentially dangerous fault in the Betic Cordilleras. Coseismic shaking can pose a high risk on the cities of Malaga and Granada. These cities were both affected during the 1884-earthquake. More than 800 casualties and several destroyed villages were reported from this event. The area is not densely populated, but agricultural zones and several holiday resorts do exist along the nearby Mediterranean coastline. Since the last earthquake has occurred in 1884 and since the fault seems to rupture roughly every 2000 years, it is questionable if the hazard is currently regarded to be high. Examples from other regions taught that the concept of "characteristic earthquakes" might not be valid at all (Stein *et al.*, 2012). If the stress release in 1884 now prevents the area from being hit by a major event in the near future must be considered an open question. However, it is proven that several events in the order of  $M6.7$  did occur.

Future research focus should now be drawn to other faults of similar length and activity, as those faults are posing significant seismic hazards, too.

### Acknowledgements

The authors thank the Spanish project CGL2006-21048-BTE and the DFG (German Science Foundation) for supporting our project Re1361/3-2. Vincenzo Spina, Arne Kaiser, Anja Schmidt, Clemens Augenstein and Christin Scur are thanked for help with the field- and lab-work. Teresa Baradjí and Pablo G. Silva helped to improve the manuscript with their constructive comments.

### References

- Alfaro, P.; Delgado, J.; Estévez, A.; López-Casado, C. (2001). *Paleoliquefaction in the Bajo Segura basin (eastern Betic Cordillera)*. *Acta Geol. Hisp.*, 36 (3-4), 233-244.

- Alfaro, P.; Bartolomé, R.; Borque, M.J.; Esévez, A.; García-Mayordomo, J.; García-Tortosa, F.J.; Gil, A.J.; Gràcia, E.; Lo Iacono, C.; Perea, H. (2012). *The Bajo Segura Fault Zone: Active blind thrusting in the Eastern Betic Cordillera (SE Spain)*, *Jour. Iberian Geol.*, 38 (1), 271-284.
- Bull, W.; McFadden, L. (1977). *Tectonic geomorphology north and south of the Garlock fault, California*, in: *Geomorphology in Arid Regions*, Proceedings of the 8th Annual Geomorphology Symposium, edited by D.E. Doehring, 115-137, State University of New York, Binghamton.
- Bull, W. (2007). *Tectonic geomorphology of mountains: a new approach to paleoseismology*, Blackwell Publishing.
- dePolo, C. M.; Slemmons, D.B. (1990). *Estimation of earthquake size for seismic hazards*, In: Krintzsky, E. L., Slemmons, D. B. (Eds.), *Neotectonics in earthquake evaluation*. *Geol. Soc. Am. Rev. Eng. Geol.*, 8, 1-28.
- Galindo-Zaldívar, J.; Gil, A.J.; Borque, M.J.; González-Lodeiro, F.; Marín-Lechado, C.; Jabaloy, A.; Ruano, P.; Sanz de Galdeano, C. (2003). *Active faulting in the internal zones of the central Betic Cordillera (SE Spain)*, *J. Geodynamics*, 36, 239-250.
- García-Mayordomo, J.; Insua-Arévalo, J.M.; Martínez-Díaz, J.J.; Jiménez-Díaz, A.; Martín-Banda, R.; Martín-Alfageme, S.; Álvarez-Gómez, J.A.; Rodríguez-Peces, M.; Pérez-López, R.; Rodríguez-Pascua, M.A.; Masana, E.; Perea, H.; Martín-González, F.; Giner-Robles, J.; Nemser, E.S.; Cabral, J.; and the QAFI Compilers Working Group (2012). *The Quaternary Active Faults Database of Iberia (QAFI v.2.0)*, *Journal of Iberian Geology*, 38 (1), 285-302.
- Grützner, C.; Reicherter, K.; Hübscher, C.; Silva, P.G. (2012). *Active faulting and neotectonics in the Baelo Claudia area, Campo de Gibraltar (southern Spain)*, *Tectonophysics*, 554-557, 127-142.
- ICA (2012). *Mapa de Andalucía Vectorial 1:10000*, Instituto de Cartografía de Andalucía, Junta de Andalucía, <http://www.juntadeandalucia.es/institutodeestadisticaycartografia/lineav2/web/>, last access 9:48, 30 October 2012.
- IGN (2012). <http://www.ign.es>, last access 15:57, 2 November 2012.
- Martínez-Díaz, J.J.; Ortuño Candela, M.; Masana, E.; García-Mayordomo, J.; Jiménez-Díaz, A. (2010a). *Alhama de Murcia Fault (1/4): Goñar-Lorca segment (ES626)*, In: García-Mayordomo et al. (eds.), *Quaternary Active Faults Database of Iberia v.2.0 - December 2011*. IGME, Madrid.
- Martínez-Díaz, J.J.; García-Mayordomo, J.; Jiménez-Díaz, A. (2010b). *Alhama de Murcia Fault (2/4): Lorca-Totana segment (ES627)*, In: García-Mayordomo et al. (eds.), *Quaternary Active Faults Database of Iberia v.2.0 - December 2011*. IGME, Madrid.
- Martínez Solares, J.M. (2011). *Sismicidad pre-instrumental. Los grandes terremotos históricos en España. Enseñanza de las ciencias de la tierra*, 19 (3), 296-304.
- Masana, E.; Martínez-Díaz, J.J.; Hernández-Enrile, J.L.; Santanach, P. (2004). *The Alhama de Murcia fault (SE Spain), a seismogenic fault in a diffuse plate boundary. Seismotectonic implications for the Ibero-Magrebian region*, *J. Geophys. Res.*, 109, 1-17.
- Masana, E.; Pallàs, R.; Perea, H.; Ortuño, M.; Martínez-Díaz, J.J.; García-Meléndez, E.; Santanach, P. (2005). *Large Holocene morphogenic earthquakes along the Albox fault, Betic Cordillera, Spain*, *J. Geodynamics*, 40, 119-133. doi:10.1016/j.jog.2005.07.002.
- Mayer, L. (1986). *Active Tectonics, chapter Tectonic Geomorphology of Escarpments and Mountain Fronts*, 125-147, National Academic Press.
- Moreno, X.; Masana, E.; Gràcia, E. (2010). *Carboneras Fault (1/2): Northern segment (ES630)*, In: García-Mayordomo et al. (eds.), *Quaternary Active Faults Database of Iberia v.2.0 - December 2011*. IGME, Madrid.
- Munsell, A. H. (1990). *Munsell soil color charts, revised ed.*, Macbeth Division of Kallmorgen Corporation, Baltimore, Maryland.
- Muñoz M.; Udías A. (1980). *Estudio de los parámetros y serie de réplicas del Terremoto de Andalucía del 25 de Diciembre de 1884 y de la sismicidad de la región Málaga-Granada*, In: Instituto Geográfico, *El Terremoto de Andalucía de 1884*, 95-139.
- Reicherter, K. (2001). *Paleoseismological advances in the Granada Basin (Betic Cordilleras, southern Spain)*, *Acta Geol. Hisp.*, 36 (3-4), 267-281.
- Reicherter K.; Jabaloy A.; Galindo-Zaldívar J.; Ruano P.; Becker-Heidmann P.; Morales, P.; Reiss, S.; Gonzales-Lodeiro, F. (2003). *Repeated palaeoseismic activity of the Ventas de Zafarraya Fault (S Spain) and its relation with the 1884 Andalusian earthquake*, *Int. J. Earth Sci.*, 92, 912-922.
- Reicherter, K.R.; Peters, G. (2005). *Neotectonic evolution of the Central Betic Cordilleras*

- (southern Spain), *Tectonophysics*, 405, 191-212.
- Rodríguez Peces, M.J.; García-Mayordomo, J. (2010). *Ventas de Zafarraya Fault (ES681)*, In: García-Mayordomo et al. (eds.), *Quaternary Active Faults Database of Iberia v.2.0* - December 2011. IGME, Madrid.
- Sanz de Galdeano, C. (1985). *La fracturación del borde sur de la Depresión de Granada (discusión acerca del ecenario del terremoto del 25-XII-1884)*, *Estud. Geol.*, 41, 59-68.
- Sanz de Galdeano, C.; Peláez, J.A.; López Casado, C. (2003). *Seismic Potential of the Main Active Faults in the Granada Basin, Pure and Applied Geophysics*, 160, 1537-1556.
- Sanz de Galdeano, C. (2012). *The Zafarraya Polje (Betic Cordillera, Granada, Spain) a basin open by lateral displacement and bending*, *J. of Geodynamics*, 64, 62-70.
- Schwartz, D.P.; Coppersmith, K.J. (1984). *Fault behavior and characteristic earthquakes: Examples from the Wasatch and San Andreas fault zones*, *J. Geophys. Res.*, 89, 5681-5698.
- Silva, P.G.; Goy, J.L.; Zazo, C.; Bardají, T. (2003). *Fault-generated mountain-fronts in southeast Spain: geomorphologic assessment of tectonic and seismic activity*, *Geomorphology*, 50 (1-3), 203-225, doi: 10.1016/A0169-555X(02)00215-5.
- Silva, P.G.; Rodríguez-Pascua, M.; Pérez-López, R.; Bardají, T.; Lario, J.; Alfaro, P.; Martínez, J.J.; Reicherter, K.; Gimenez, J.; Giner-Robles, J.; Azañon, J.M.; Goy, J.L.; Zazo, C. (2009). *Catalogacion de los efectos geologicos y ambientales de los terremotos en España en la Escala ESI-2007 y su aplicacion a los estudios paleosismologicos*, *Geotemas*, 6, 1063-1066.
- Stein, S.; Geller, R.J.; Liu, M. (2012). *Why earthquake hazard maps often fail and what to do about it*, *Tectonophysics*, 562-563, 1-25.
- Wells, D.L.; Coppersmith, K.J. (1994). *New Empirical Relationships among Magnitude, Rupture Length, Rupture Width, Rupture Area, and Surface Displacement*, *Bulletin of the Seismological Society of America*, 84 (4), 974-1002.